Acute lymph node slices are a functional model system to study immunity ex vivo

Maura C. Belanger*[‖], Andrew W.L. Kinman*[‖], Megan A. Catterton*[‖], Alexander G. Ball[†‖], Benjamin D. Groff*[‖], Stephanie J. Melchor[†‖], John R. Lukens[#‖], Ashley E. Ross[‡], and Rebecca R. Pompano*[‖ϕ‖]

Department of Chemistry
Carter Immunology Center
University of Virginia
McCormick Rd.
PO Box 400319
Charlottesville, VA USA 22904

[‖] Corresponding author
Email: rrp2z@virginia.edu
Phone: 1-434-982-1825

* Department of Chemistry, University of Virginia College of Arts and Sciences, Charlottesville, VA 22904
[‖] Carter Immunology Center, University of Virginia, Charlottesville, VA 22904
[†] Department of Microbiology, Immunology and Cancer Biology, University of Virginia School of Medicine, Charlottesville, VA 22904
Department of Neuroscience and Center for Brain Immunology and Glia (BIG), University of Virginia School of Medicine, Charlottesville, VA 22904
[‡] Department of Chemistry, University of Cincinnati, Cincinnati, OH 45220
[ϕ] Department of Biomedical Engineering, University of Virginia School of Engineering and Applied Sciences, Charlottesville, VA 22904

Abstract:

A major hub of adaptive immunity is the lymph node, which has a highly organized and dynamic structure. Most techniques currently used to study the lymph node ex vivo begin by reducing the tissue to a cell suspension, thus losing the spatial organization, or fixing the tissue, thus losing the ability to make measurements over time or after stimulation. Live tissue slices offer the potential to retain spatial complexity and provide the dynamic accessibility of traditional in vitro measurements, but this approach has not been rigorously validated for murine lymph node tissue. Here we describe a systematic characterization of live murine lymph node slices as a platform to study immunity. Live lymph node slices maintained the expected spatial organization and were comprised of the expected cell populations. Slices collected under optimized conditions were comparable to cell suspensions both in terms of 24-hr viability and inflammation. Slices processed protein antigens and responded to T cell receptor cross-linking with expected surface marker expression and cytokine secretion. Interestingly, IFN-γ but not IL-2 secretion from slices was higher than from cell suspensions after both CD3 and R848 stimulation. Furthermore, slices from vaccinated animals responded to ex vivo antigen challenge with antigen-specific cytokine secretion. In summary, lymph node slices provide an experimental platform that maintains spatial organization and temporal dynamics, while allowing for controlled stimulus-response experiments with multiple parallel read-outs. We anticipate that tissue slices may serve as a versatile tool to investigate immune functions within the lymph node.

Introduction:

Events in the LN determine how well we fight infections and respond to vaccines, whether a nascent tumor is recognized and destroyed, and whether our own tissues remain safe from autoimmunity. These immune responses arise in large part from exquisite spatial organization of cells and proteins in the lymph node.[1–3] The structure of a lymph node can be roughly divided into an outer cortex containing B cell follicles, a T cell zone, or paracortex, and an inner medulla.[1,4] During an immune response, cells in these regions communicate through both physical contact and secreted signals. Diffusion and the formation of gradients of secreted cytokines through the extracellular matrix generate orchestrated cell migration,[5–7] and the local concentration of cytokines and other signals can drive strong positive feedback and divergent outcomes.[8] All of these features suggest that the organization of the node may be essential to its function,[2,9,10] and indeed, many similarly complex non-linear biological systems are exquisitely sensitive to spatial organization.[11]

Investigating the function of the lymph node with high spatial, temporal, and chemical resolution within a realistic microenvironment is challenging with existing experimental systems. Recent technological advances in immunological analysis have focused significantly on high-content single cell data using flow cytometry or mass cytometry,[12,13] analysis of single-cell secretion and gene expression using microfluidics,[14–20] and on bulk measurements such as metabolomics[21] and live cell metabolic analysis.[22] However, these cannot provide information on LN organization. Complementing this work, live in vivo imaging was developed over 15 years ago and continues to provide impressive insight into the dynamics of cell and tissue-level behavior in the native environment.[23–27] Yet, it is challenging to experimentally manipulate tissues in vivo without prior genetic modification (e.g. optogenetics) or invasive injection. Approaches that retain the tissue's spatial organization via fixation have been of increased interest towards understanding the biological relevance of distinct cellular subpopulations.[28–30] These methods are very powerful, yet a single approach that maintains the biological complexity of the organ while providing dynamic experimental access close to that of traditional cell cultures is still largely missing from the immunologist's toolbox.[31]

Live ex vivo slices of lymph node tissue may provide a necessary middle-out approach, in a manner complementary to in vitro and in vivo work. Unlike in vitro cell culture, slices preserve the extracellular microenvironment and any stromal and matrix-bound signals, which are essential to proper cellular positioning and motility.[2,6,32–34] Furthermore, all cell types are retained in their correct ratios, whereas standard tissue dissociation (crushing and filtering) selectively depletes matrix-bound populations such as dendritic cells.[35] Decades of work with brain slices[36–39] set a precedent for both acute[38,40] and long-term experimentation,[41] which informed protocols for other tissues such as the pancreas,[42] liver,[43] lung[44] and heart.[45] In the field of immunology, slices of the thymus have been used extensively to study T cell development.[46,47] Live spleen[48,49] and tonsillar[50–52] slices were demonstrated 20 years ago, and continue to be a valuable tool to study immune functions. Many of the reported uses of live lymph node tissue slices have been to study T cell motility.[53–57] Using tissue slices allows for multiple time points to be measured within the same tissue and so the response to a stimulus can be tracked easily over time.[51,58–62] These slices also allow for precise probing of the organ interior and the effects of inter-organ communication; once removed from the organism, precise quantities of stimulants or other organ samples can be added ex vivo without other confounding factors.[63,64]

At this time, unanswered questions regarding the viability, level of inflammation, and retention of function appear as potential obstacles to the broad adoption of live lymph node slices. To address this issue, here we describe a systematic evaluation of the procedures surrounding the slicing, handling, and analyzing of live murine lymph nodes in short-term cultures, towards establishing lymph node slices as a reputable experimental platform. We comprehensively assess 24-hr viability, the extent of inflammation due to slicing, and retention of acute function. Finally, we validate the use of acute murine lymph node slices to quantify antigen-specific T cell responses ex vivo.

Materials and Methods:

Generating lymph node tissue slices

All animal work was approved by the Institutional Animal Care and Use Committee at the University of Virginia under protocol #4042, and was conducted in compliance with guidelines the Office of Laboratory Animal Welfare at the National Institutes of Health (United States). Male and female C57BL/6 mice ages 6-12 weeks (Jackson Laboratory, USA) were housed in a vivarium and given water and food ad libitum. On the day of the experiment, animals were anesthetized with isoflurane followed by cervical dislocation. The axial, inguinal, and brachial lymph nodes were removed quickly but carefully and cleaned of any fat. It was critical to harvest the organ without stretching, tearing, or poking it with tweezers. This required a more delicate technique than is used for collection of tissues that will be passed through a filter prior to cell culture. Lymph nodes were placed in ice-cold DPBS without calcium or magnesium (Lonza, Walkersville MD, USA, #17-512F) supplemented with 2 % heat-inactivated fetal bovine serum (FBS, Gibco, Fisher Scientific, 100 % US Origin, 1500-500 Lot 106B14). Lymph nodes were embedded in 6 % w/v low melting point agarose (Lonza, Walkersville MD, USA) in 1X PBS. Agarose was melted in a microwave and allowed to cool until the temperature was comfortable in the hand. Further optimization showed that maintaining the melted agarose at 50 °C in a water bath after microwaving provided a more reproducible approach. Liquid agarose was poured into a 35 mm Petri dish; lymph nodes were embedded in the liquid agarose close to the bottom of the dish, oriented to allow for the largest cross-section when slicing. The dish was then rested at room temperature for approximately 2 minutes and allowed to harden on ice for the next 3 minutes. Once hardened, a 10 mm tissue punch (World Precision Instruments) was used to extract a section of agarose containing the lymph node. The block was flipped so the node was at the top of the section and glued onto a small mounting stage with Duro® Super Glue (cyanoacrylate) and immediately submerged in a buffer tray containing ice-cold 1X PBS unless otherwise noted. Up to 6 lymph nodes were mounted on a single stage and sliced simultaneously.

A Leica VT1000S vibratome (Bannockburn, IL, USA) set to a speed of 90 (0.17 mm/s) and frequency of 3 (30 Hz) was used to slice 300-µm thick sections. A fan-shaped paint brush was used to remove the slices. Slices were immediately placed in a 6-well plate containing 3 mL per well of “complete

RPMI": RPMI (Lonza, 16-167F) supplemented with 10 % FBS (VWR, Seradigm USDA approved, 89510-186) 1x L-glutamine (Gibco Life Technologies, 25030-081), 50 U/mL Pen/Strep (Gibco), 50 µM beta-mercaptoethanol (Gibco, 21985-023), 1 mM sodium pyruvate (Hyclone, GE USA), 1x non-essential amino acids (Hyclone, SH30598.01), and 20 mM HEPES (VWR, 97064-362). Slices were rested in a sterile incubator at 37 °C with 5 % CO_2 for at least one hour prior to use.

Activation of cell suspensions and tissue samples

Primary lymphocyte cell cultures were prepared by passing 6 peripheral nodes (axial, brachial, and inguinal) through a single 70-µm nylon mesh filter (Thermo Fisher, USA) with the rubber tip of the plunger from either a 1- or 3-mL syringe. Cells were plated in a 96-well cell-culture treated plate (Costar, VWR, USA) at a density of $1x10^6$ cells/mL in a 300 µL final volume. To obtain inflamed lymphocytes as positive controls, aluminum hydroxide gel adjuvant (Alhydrogel®, 10 mg/mL alum, Invivogen) was added to the wells for a final concentration of 1 mg/mL alum. Cells were cultured for 3.5 hours in a cell culture incubator (37 °C, 5% CO_2) and prepared for flow as described below.

To compare activation of slices versus cell suspensions, peripheral lymph nodes were randomly assigned to be sliced or crushed for lymphocyte culture. For the sliced condition, nodes were sliced 300 µm thick and each slice was placed into 500 µL complete media. For lymphocyte culture condition, nodes were crushed through a filter as described above. Lymphocyte suspensions were cultured in 500 µL aliquots at cell densities matched to tissue slice samples, where 1X culture was 1.7 $x10^6$ cells/mL, and 2X culture was 3.4 $x10^6$ cells/mL. Slices and lymphocyte cell culture were incubated for 20 hours at 37 °C, 5% CO_2, with anti-mouse/human CD3Ɛ (BioLegend, clone: 145-2C11, Purified grade) at 1, 0.5, or 0 µg/mL, with R848 (Resiquimod, InvivoGen, San Diego, CA) at 10 1, 0.1, or 0 µg/mL, or F(ab')2 goat anti-mouse IgM (µ chain specific, Jackson ImmunoResearch) at 10 µg/mL.

Flow cytometry

To prepare samples for flow cytometry, tissue slices were separated from the surrounding agarose through careful mechanical manipulation with a paint brush; individual tissue slices or groups of slices were then crushed through a 70-µm nylon mesh filter (Thermo Fisher, USA) using the rubber tip of

a 1 or 3 mL syringe plunger to generate cell suspensions. Unsliced lymph nodes were similarly crushed through 70-µm filters, according to standard methods, for comparison. Cell suspensions were stained with Pacific Blue-B220, Brilliant Violet 421-CD3, Alexa Fluor 488-CD80, PE-CD11c, PE-Cy7-CD69, APC-Cy7-CD4 (all from Biolegend, USA, details provided in Table S1) and DilC1 (Thermo Fisher, USA). After staining, 2 µM propidium iodide (PI, Sigma Aldrich, USA) was added. Stained samples were washed and resuspended in 500 µL of 1x PBS with 2% FBS (flow buffer). Antibody compensation controls were run with OneComp eBeads™ (eBiosciences, USA) according to manufacturer protocol. Viability compensation controls, including PI and DilC1, were run on primary lymphocyte populations. PI controls were run with mixed live and killed cells; cells were killed with 35% ethanol for 10 minutes at room temperature. Live cells were stained with DilC1 for 30 minutes at 4 °C, washed and mixed with unstained live cells in a 1:1 ratio to act as a single stain compensation control. Stained suspensions were analyzed on a CyAn APD LX cytometer (Beckman Coulter, USA) unless otherwise noted. Analysis was completed using FlowJo 7 or FCS Express as noted.

To estimate the number of cells obtained from either individual or pooled slices by flow cytometry, samples were run on a BD FACSCalibur instrument with a flow rate of 1 µL/sec. Data was collected for 10,000 events within a lymphocyte scatter gate. The time of running the sample was recorded, from which the run volume was calculated. Using this volume and the number of lymphocytes in the analyzed sample, we calculated the number of lymphocytes per volume in each sample.

ELISA

Culture supernatant was collected and analyzed by sandwich ELISA for the cytokines IFNγ, IL-2, IL-4, and TNFα. A high-binding plate (Corning Costar 96 well ½ area, #3690; Fisher Scientific) was coated with 1 µg/mL anti-IFNγ XMG1.2, 1 µg/mL anti-IL-2 JES6-1A12, ELISA MAX capture anti-IL-4 (previous antibodies from BioLegend) or capture TNFα (R&D systems, cat: DY410-05) in PBS overnight at 4°C, then washed. All washing steps were performed in triplicate with 0.05% Tween-20 in PBS. Wells were blocked for 2 hours with 1% BSA and 0.05% Tween-20 (Fisher Scientific) in PBS (block solution). Serial dilutions of recombinant murine IFNγ, IL-2 (Peprotech, Rocky Hill, NJ), IL-4 (ELISA MAX standard, BioLegend) and TNFα (R&D Systems) were prepared in a 1:1 v/v mixture of block solution and complete

media, and supernatant samples were diluted 1:1 v/v with block solution. Samples were added to the plate in duplicate and incubated for 2 hours, then washed. Biotinylated anti-IFNγ R46A2 (0.5 µg/mL), anti-IL-2 JES6-5H4 (1 µg/mL), ELISA MAX detection anti-IL-4 (BioLegend), or detection TNFα (R&D Systems) were prepared in blocking solution and added to the plate. Avidin-HRP (1X) (Fisher Scientific) in blocking solution was added to the plate and incubated for 30 minutes, then washed. Plates were developed using TMB substrate (Fisher Scientific), stopped with 1M sulfuric acid (Fisher Scientific), and absorbance values were read at 450 nm on a plate reader (CLARIOstar; BMG LabTech, Cary, NC). To determine concentration of sample solutions, calibration curves were fit in GraphPad Prism 6 with a sigmoidal 4 parameter curve (Eq. (1)), where X is concentration, Y is absorbance, min and max are the plateaus of the sigmoidal curve on the Y axis, and HillSlope describes the steepness of the slope.

$$\mathrm{Y} = \min + (\mathrm{X}^{\mathrm{HillSlope}}) \times \frac{(\max - \min)}{(\mathrm{X}^{\mathrm{HillSlope}} + \mathrm{EC50}^{\mathrm{HillSlope}})} \quad (1)$$

Limit of Detection (LOD) was calculated from the average of the blank + 3x standard deviation of the blank.

Inflammatory Gene Expression Array

Axial, brachial, and inguinal lymph nodes from four mice were mixed and randomly distributed into two groups: 12 nodes for slicing and 12 nodes for cell suspensions. Approximately 24 slices were collected as described above and cultured individually at 37 °C with 5% CO2 overnight. Cell suspensions were generated by passing the lymph nodes through a 70-µm filter. Cells were pooled and resuspended at 0.86 x10^6 cells/mL (mean cellular density matched to the lymph node slices) then cultured overnight. Samples were flash frozen and stored at -80 °C until RNA could be isolated.

RNA was isolated using a RNeasy Mini Kit according to manufacturer instructions (Qiagen, USA). Briefly, pooled tissue samples were homogenized in lysate buffer; cells were vortexed in lysate buffer and passed through a 20-gauge needle to generate a homogenized sample. Lysates were mixed with 70% ethanol and passed through the supplied filter kit to obtain genetic material. To remove genomic DNA from the sample, 1 µg RNA was added to 1 U/µL DNase (Invitrogen, USA) in DNase reaction buffer. The digestion was run for 15 min at room temperature and stopped with 25 mM EDTA and heated to 65

degrees C for 10 min. An Accuris qMax cDNA synthesis kit was used to generate the cDNA. Reaction buffer, qMax reverse transcriptase, RNA and water were incubated at 42 degrees for 30 minutes. The reaction was stopped by heating to 85 degrees for 10 minutes.

A RT^2 profiler array for mouse inflammatory cytokines and receptors (Qiagen, USA) was used according to manufacturer recommendations to measure the expression of 84 inflammatory genes (Table S2). SYBR Green was used as the reporter and the reaction was run for 40 cycles on a QuantStudio 6 PCR instrument (Thermo Fisher, USA). Genes that were detected on or after cycle 35 were considered not expressed. Of the expressed genes, the average relative expression was determined based on the average expression of 5 housekeeping genes (Table S2) Because all samples in each group were pooled for analysis, two thresholds were defined for significant differential expression, two and three standard deviations from the mean differential expression.

DQ-OVA culture of lymph node slices

Slices were collected as above and randomly assigned to live culture or fixation. Live slices were cultured with OVA protein solution (1 µg/mL DQ-Ovalbumin (OVA, Thermo Fisher, USA) and 9 µg/mL purified OVA (InvivoGen, USA)) or vehicle control, in 500 µL supplemented RPMI. Killed control slices were fixed in formalin (4% formaldehyde, Protocol, USA) for 1 hour at 37 °C with 5% CO_2, then incubated with OVA protein solution. Slices were incubated for 24 hours at 37 °C, 5% CO_2, and images were collected at 1,2,4,8 and 24 hours.

Antigen-specific interactions in lymph node slices

Spleens were collected from Rag2/OT-II female mice (Taconic Biosciences) aged 6-10 weeks following isoflurane anesthesia and cervical dislocation. Splenocytes were isolated using a 70-µm pore size nylon filter (Fisher Scientific, USA), and the filter was washed with sterile 1x phosphate buffer saline (PBS) supplemented with 2% v/v fetal bovine serum (FBS, VWR, USA). Cell density was determined through trypan blue exclusion. Using a CD4+ T cell enrichment kit (StemCell Technologies, USA), CD4+ T cells were isolated from bulk splenocytes by negative selection. OTII CD4+ T cells ($0.5x10^6$ cells: 200 µL at $2.5x10^6$ cells/mL) were intravenously injected into 8 female C57Bl/6 mice. The following day, the

C57Bl/6 mice were vaccinated with 50 µg of OVA protein in either 200 µL of Alum 50:50 v/v PBS or PBS alone. Vaccinated mice were humanely euthanized on days 1,4 and 7 after vaccination, and lymph nodes were harvested and sliced. Slices were cultured overnight in complete media supplemented with 10 µg/mL OVA protein (Invivogen) or PBS. After overnight culture, the supernatant was collected for cytokine analysis using ELISA and the slices immunostained and imaged.

Immunofluorescent staining and imaging of lymph node slices

Slices were stained according to previously published procedures.[61] Briefly, slices were placed on a Parafilm® covered surface and a washer was placed on top. Samples were treated with blocking solution (anti-CD16/32) for 20 minutes in a cell culture incubator. Antibody cocktail was added to the blocking solution and samples were incubated for an additional 1 hour. Slices were then washed in sterile 1x PBS for at least 30 minutes in a cell culture incubator.

Unless otherwise noted, imaging was performed on a Zeiss AxioZoom upright macroscope with a PlanNeoFluor Z 1x/0.25 FWD 56mm objective, Axiocam 506 mono camera and HXP 200 C metal halide lamp (Zeiss Microscopy, Germany). Images were collected with Zeiss Filter Sets 38 HE (Ex: 470/40, Em: 525/50), 43 HE (Ex: 550/25, Em: 605/70); 64 HE (Ex: 587/25, Em: 647/70); and 50 (Ex: 640/30, Em: 690/50). Image analysis was completed using ImageJ software 1.48v.[65]

Results:

Lymph node slices preserve spatial organization

We developed a protocol for slicing lymph node tissue that was informed by well-established procedures for slicing brain, another delicate tissue, and by prior work with lymphoid tissues.[46,59,66] In brief, LNs were gently isolated from the animal, embedded in agarose for physical support, and sliced on a vibratome. LN slices were immediately immersed in to culture media to rest until further processing or experimentation. A detailed experimental protocol is provided in the Methods. In this first section, we highlight some of the key aspects of working with lymph node slices prior to describing the optimization and validation of the method.

One of the primary reasons to work with intact tissue rather than cell culture is the preservation of spatial organization. Indeed, the structure of the lymph node was retained in these live, thick slices in the absence of fixation. Live tissue slices from naïve mice contained distinct B cell regions and lymphatic vasculature/vessels with a distribution that was consistent with those reported from in vivo and immuno-histochemical studies (Figure 1 a).[46,30,67–69] These geographical landmarks were readily visualized using widefield microscopy after live immunofluorescence staining.[61] As these are thick slices of tissue (300 µm), cellular composition and distribution varies between consecutive slices and even within a single slice (Figure S1). Ex vivo slices could also be used to visualize the distribution of draining antigen after in vivo vaccination, e.g. with rhodamine-conjugated ovalbumin (OVA) protein (Figure 1 b-d). Both localization in individual cells (Figure 1b) and draining of soluble antigen via the lymphatic and sinus structure (Figure 1 c-d) were visible without fixing the tissue.

While the images described above were collected at low magnification, live tissue slices are also compatible with high resolution microscopy techniques. By using confocal microscopy, we were able to visualize individual cells within the branching lymphatic network (Figure 1e). Second harmonic imaging of the collagen network within the LN slice (Figure 1f) highlighted the dense collagen network that persists throughout the lymph node, consistent with other examples of live two-photon imaging of the lymph node.[70–72]

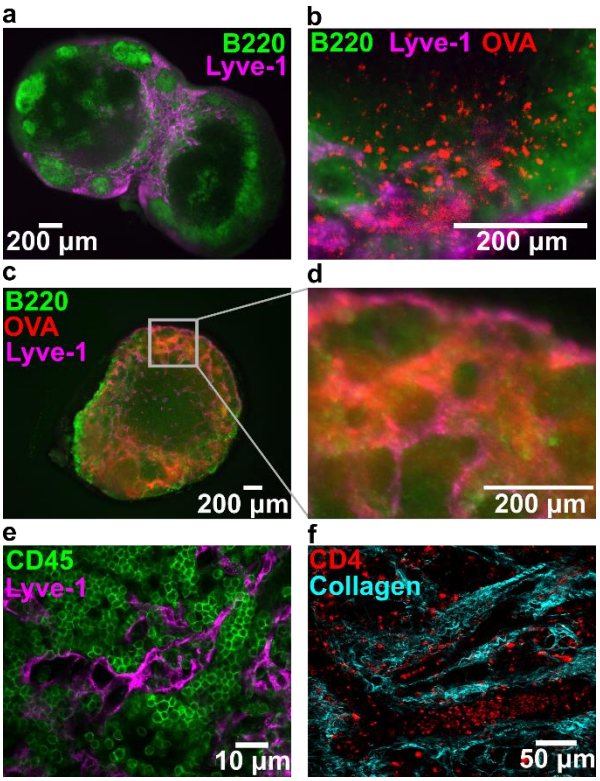

Figure 1: Key structural features remain intact in thick lymph node slices, allowing for analysis at both the tissue and cellular levels. (a) Slice labeled with anti-B220 (FITC, green) and anti-lyve-1 (eFluor660, purple) revealed key structural features of the lymph node. (b-d) Slices from an OVA (rhodamine labelled, red)-immunized mouse, labeled as in (a). (b) Rhodamine-OVA was visible inside of cells within the T cell rich (B220-dim) region of the lymph node. (c) Rhodamine-OVA entering the lymph node through the lymphatics. (d) Inset of (c) showing colocalization of draining lymphatics and OVA protein. (e) High-definition image collected by confocal microscopy. Slice labelled with anti-CD45 (AlexaFluor488, green) and anti-lyve-1 (eFluor660, purple). (f) Image of lymph node slice collected by two-photon microscopy, showing CD4 positive T cells within the collagen matrix (second harmonic imaging). A detailed procedural description for each panel is provided in the SI Methods.

Cellular phenotyping in single LN slices

To enable quantitative cellular phenotyping and analysis of viability, we first determined the minimum number of lymph node slices required for flow cytometry. Flow cytometric analysis of single murine tissue slices has been reported for thymus but not for lymph node.[63] Varying numbers of slices were crushed, pooled, and counted by flow cytometry. We found that a single slice provided sufficient cell counts to collect flow cytometric data (*Figure 2* a, i), and all subsequent analyses were performed on single slices unless otherwise noted. In separate experiments, manual counting showed that naïve lymph nodes contained 1.7 ± 0.8 x10^6 lymphocytes per node (mean ± std dev, n = 30 nodes from 5 female mice

aged 6-12 weeks). We typically obtain two or three 300-µm-thick slices per node; yielding an estimated ~ 0.5–1 x10^6 lymphocytes per slice.

We examined the viability and early activation state of specific cell populations within lymph node slices. Live cells were identified using PI exclusion, and the remaining cells were separated into dead (PI^{high}, $DilC1^{low}$) and apoptotic (PI^{high}, $DilC1^{high}$) populations according to signal from the mitochondrial membrane potential dye DilC1 (Figure 2 b). Live cells were phenotyped by surface markers for cell type (Figure 2 c,e,g)[73] and early-stage activation: CD69 for CD4+ T cells and CD80 for B cells and CD11c-expressing cells, which include dendritic cells (DCs) (Figure 2 d,f,h).[74–76] On average, the cell suspension obtained from a single C57Bl/6 lymph node slice was comprised of 48% CD3+ T cells, 47% B cells, and ~ 1% CD11c+ (Figure 2 j). The low percentage of CD11c+ cells is expected because these cells are most likely lost to the membrane during crushing.[67] The CD3+ population consisted of an average of 45% CD4+ and 50% CD4-. There was large heterogeneity in cellular composition between individual slices, consistent with the complex 3-dimensional structure of this organ.

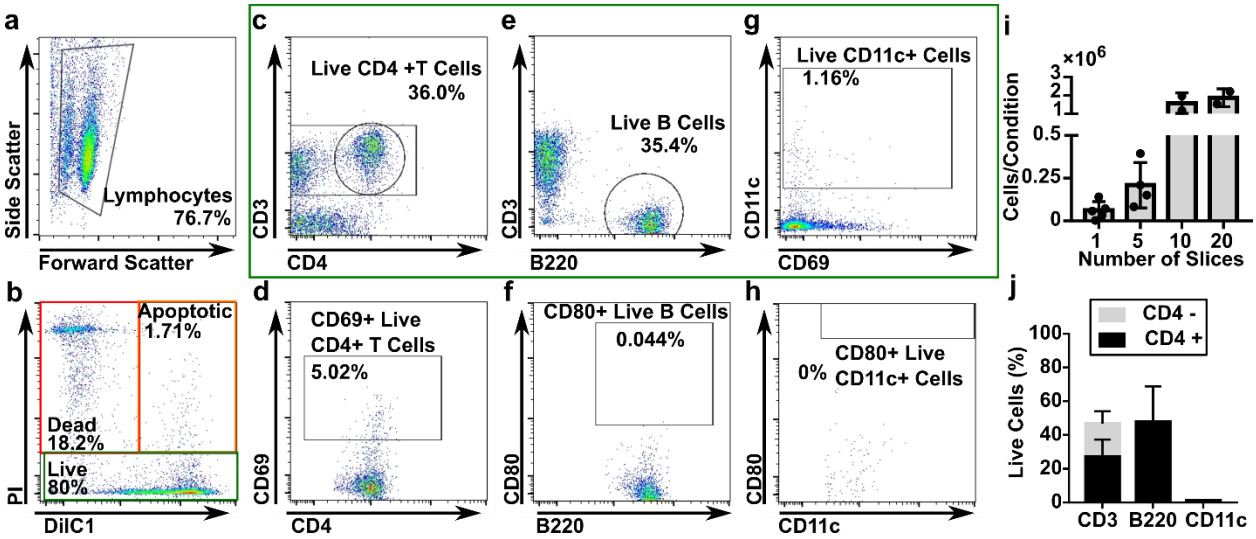

Figure 2: Flow cytometric analysis of single lymph node slices. Representative flow plots from a single naïve slice showing scatter (a), viability (b), T cell, B cell, and CD11c+ cell phenotyping (c,e,g, respectively) and activation markers on T cells, B cells and CD11c cells (d,f,h, respectively). (i) Determination of minimum number of slices required for analysis. The indicated number of slices was combined and crushed into a single sample, analyzed, and the total cell number was estimated. Each dot indicates one sample. (j) Average phenotypic break-down of individual lymph node slices. The average slice was equally distributed between B cells (48±21%) and CD3+ T cells (47±17%), with very few

CD11c+ cells collected (1±0.4%); exact composition varied between slices. Bars show mean ± standard deviation from N=7 slices for phenotypic data.

Single 300-μm LN slices had similar viability overnight as lymphocyte suspensions

Next, we optimized the conditions for slicing in terms of its impact on viability and inflammatory state of the tissue. For reference, we compared cells collected from tissue slices to cells collected directly from intact lymph nodes by the conventional method of crushing through a filter (Figure 3 a). First, we determined the appropriate thickness for murine lymph node slices (Figure 3 b); the minimal slice thickness for a given tissue depends on its mechanical strength, while an upper bound is set by its rate of oxygen consumption.[77] Lymph node slices collected at 100 μm were usually torn, and this thickness was not considered further. 200-μm-thick slices were intact but sometimes mechanically distended (stretched); consistent with this, these slices were diminished in initial viability compared to 400-μm slices. There was no significant difference in initial or 24-hr viability between 300-μm and 400-μm slices, so 300 μm was selected to provide more slices per node. Overall, the percentage of live cells in slices was similar to that of cell culture suspensions over this time period. These results demonstrate that the act of slicing did not significantly decrease the viability of the samples compared to crushing.

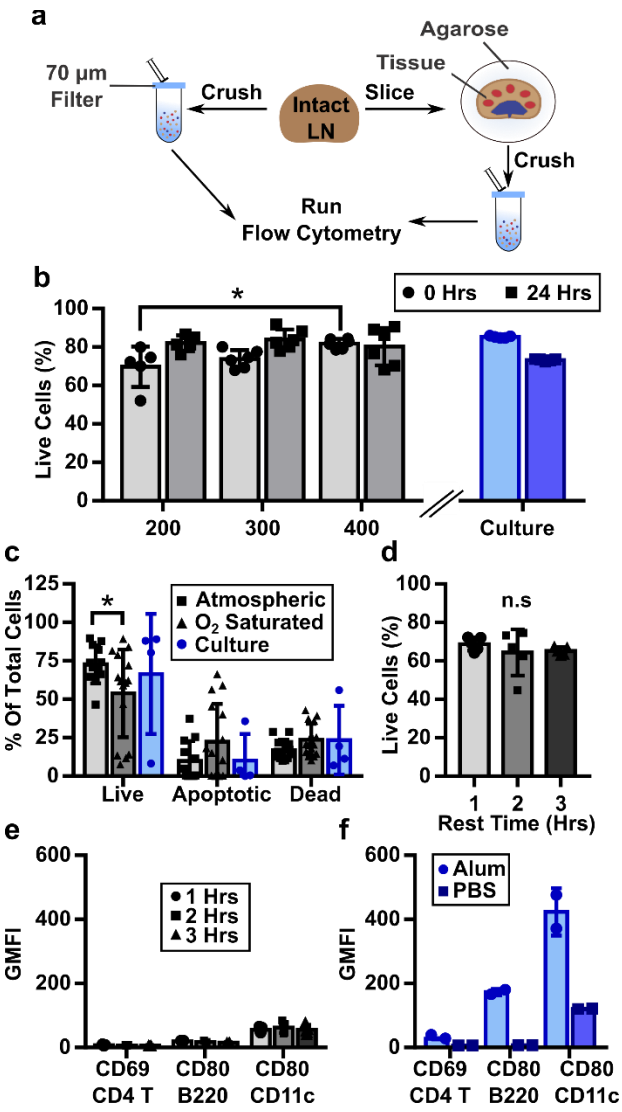

Figure 3: Optimizing parameters for LN slicing. (a) Schematic showing experimental work flow: Intact LNs were either passed through a 70-µm filter or embedded in agarose, sliced, cultured, and then passed through a filter. (b) Tissue thickness had a slight effect on initial viability, as 200-µm thick slices were less viable than 400-µm thick slices. No significant differences were seen between thicknesses after 24 hours of culture. The viability of tissue slices was comparable to that of cell culture. (c) Slicing LNs in O_2-saturated media caused damage to the cells as indicated by a decrease in the live and increased spread in the apoptotic populations. (d) Viability was unchanged over short recovery times. (e) The intensity of inflammation markers remained low over short recovery times and was much lower than (f) alum-treated in vitro lymphocyte cultures used as a positive control. 2-way ANOVA with multiple comparisons *$p<0.05$, n.s. $p>0.05$.

Selection of slicing conditions to minimize activation markers

Next, we considered the content and oxygenation of the media used during slicing. Inclusion of proteins in the chilled slicing media (2% fetal bovine serum (FBS) in PBS) did not improve viability (Figure S2), so PBS was used for simplicity. Oxygenation of slicing media is essential for brain slices, and this convention has been propagated through many other tissue slicing protocols.[46,66,59,78,79] However, lymph nodes, and many other tissues, are thought to be mildly hypoxic in vivo.[80] We hypothesized that hyperoxia may not be needed during slicing of LN tissue. To test this hypothesis, we sliced tissue in atmospheric and oxygen-saturated environments. Slices collected in oxygen-saturated media showed a small but significant decrease in the live population compared to those sliced under atmospheric conditions and trended towards a greater apoptotic population (Figure 3 c). CD80 expression was also increased on CD11c positive cells from these slices (Figure S3). From these data we concluded that a hyperoxic environment during slicing was not beneficial to the health of the lymph node tissue, and going forward, all slices were collected in 1x PBS without oxygen bubbling. We note that these results were collected on skin-draining lymph nodes, and we cannot exclude the possibility that lymph nodes from other areas of the body may require different handling.

We considered the concern that the act of slicing has the potential to induce rapid, non-specific inflammation due to mechanical damage. Slices of many organs are “rested” for one or more hours after collection to allow any effects of cutting to dissipate,[45,81,82] and we tested slices in this window for viability and upregulation of inflammatory markers. We found no significant difference in viability over a period of 1 – 3 hr after slicing (Figure 3 d), nor any increase in the fluorescence intensities of the activation markers CD69 on CD4+ T cells and CD80 on B cells and CD11c+ cells (Figure 3 e). Furthermore, the CD69 and CD80 intensities from slices were much lower than from lymphocytes were treated in vitro with alum as a positive control (Figure 3 f). Based on these data, we determined that a 1-hour rest is sufficient post-slicing; shorter times may also be acceptable but were not tested. We speculate that the lack of measurable inflammation in response to the mechanical damage of slicing may be due to the rapid dilution of “danger signals” from the cut faces of the slice into the large volume of slicing media. In

summary, lymph node slices collected in normoxic saline and rested for one hour displayed high viability and minimal markers of nonspecific activation.

Inflammatory gene expression was low and similar between sliced and crushed lymph node.

To further investigate the possibility of inflammation due to slicing, the expression of 84 key inflammatory genes (Table S2) was analyzed by RT-PCR array for lymph node tissue slices versus conventional lymphocyte cultures. Samples were cultured overnight prior to analysis, to allow time for any delayed response or slow-acting inflammatory signals from the process of slicing. Consistent with the fact that these were samples from naïve animals, many genes in the inflammatory gene array were not expressed in either sample (27 genes) (Figure 4 a). For the 57 genes that were detectably expressed in one or both sample types, differential expression was determined by calculating the mean relative expression and setting thresholds at one and two standard deviations from the mean. Using the least stringent threshold (1 standard deviation) for differential expression, there were 39 genes that were not differentially expressed between slices and cell culture (Figure 4 b, blue points). Of the 18 differentially expressed genes, 9 were related to chemokines and their receptors (Figure 4 c). We hypothesize that this difference may be related to the maintenance of the stromal cells or extracellular matrix in the sliced tissue. When we increased the threshold from one standard deviation to two, 7 genes were reclassified as not differentially expressed (Figure 4, light orange); these were included in the preceding discussion to provide a more comprehensive analysis of any potential inflammatory effects. Based on the overall low levels of inflammatory gene expression and the similarity between tissue slices and cell suspensions, together with the low levels of activation markers (Figure 3), we conclude that the process of slicing does not cause appreciable inflammation of the tissue. These data are consistent with results from tumor slices that found few changes in gene expression caused by the act of slicing.[83]

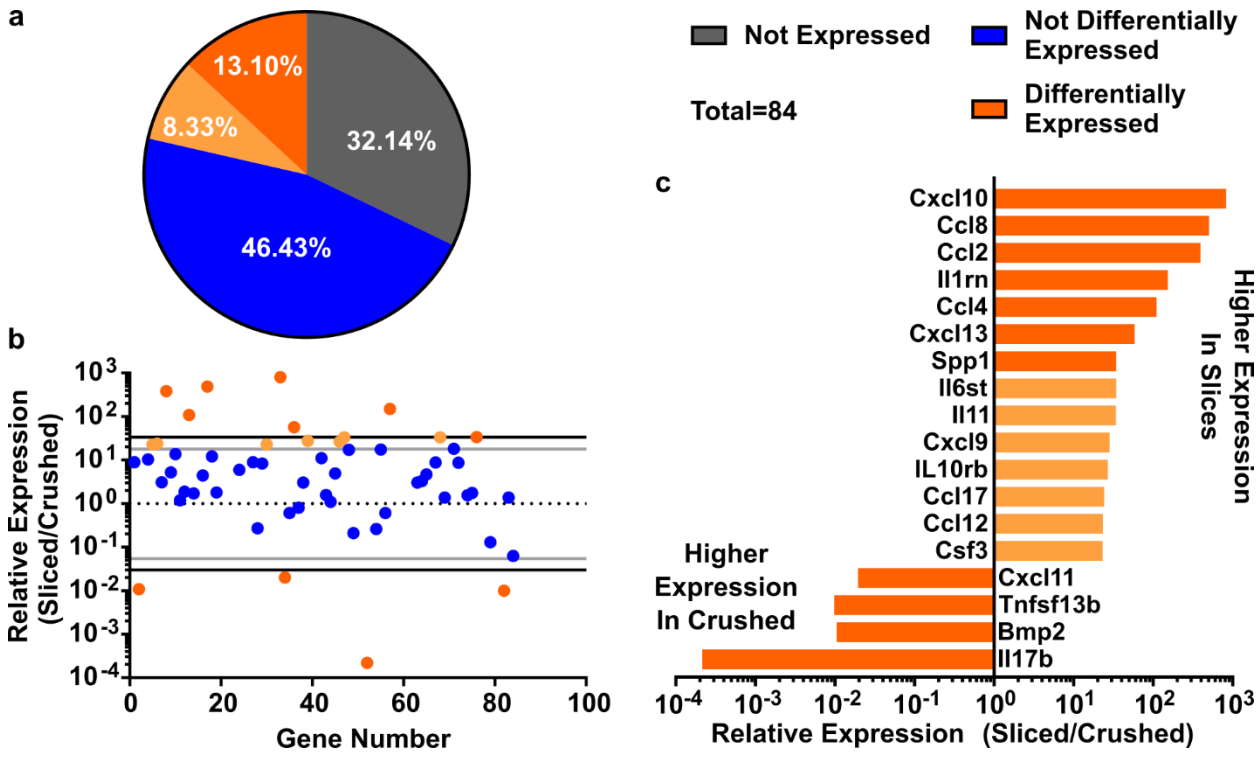

Figure 4: Similarly low expression of inflammatory genes in slices and cell suspensions from naïve murine lymph nodes. (a) Of the 84 genes, investigated 32% were not expressed in either condition, 46% were expressed but not differentially expressed, and 13-21% were differentially expressed. Differential expression was determined by setting a threshold at 1 or 2 standard deviations from the mean relative expression of expressed genes (light and dark orange, respectively). (b) Expressed genes were categorized by the two thresholds: 2 stdev (black lines) or 1 stdev (grey lines). Seven genes were different between the thresholds. For full gene list refer to SI Table 1. (c) Identification of differentially expressed genes. The 7 identified by the more lenient threshold are indicated by the lighter orange bars. Data from pooled samples from N=3 mice, 9 crushed nodes, 30 slices.

Lymph node slices processed whole-protein antigen and responded to cellular stimulation

An exciting application of lymph node slice culture is to measure the response of the intact tissue to ex vivo stimulation, with all cell types and structures present and correctly localized. We were particularly interested in the function of antigen-presenting cells because appropriate antigen recognition is required to initiate adaptive immune responses. We tested the ability of antigen-presenting cells to process whole-protein antigen by incubating live slices with DQ-Ovalbumin, a modified form of OVA that becomes fluorescent upon proteolytic cleavage. Repeated fluorescent imaging revealed time-dependent uptake and processing of the whole-protein antigen by cells in lymph node slices. Mean DQ-OVA intensity was significantly greater in live slices than in fixed slices after just two hours (Figure 5 a). DQ-

OVA signal followed a spatial distribution that was consistent with the sinuses and lymphatics (Figure 5 b), similar to the pattern observed for in vivo antigen drainage (Figure 1 d).

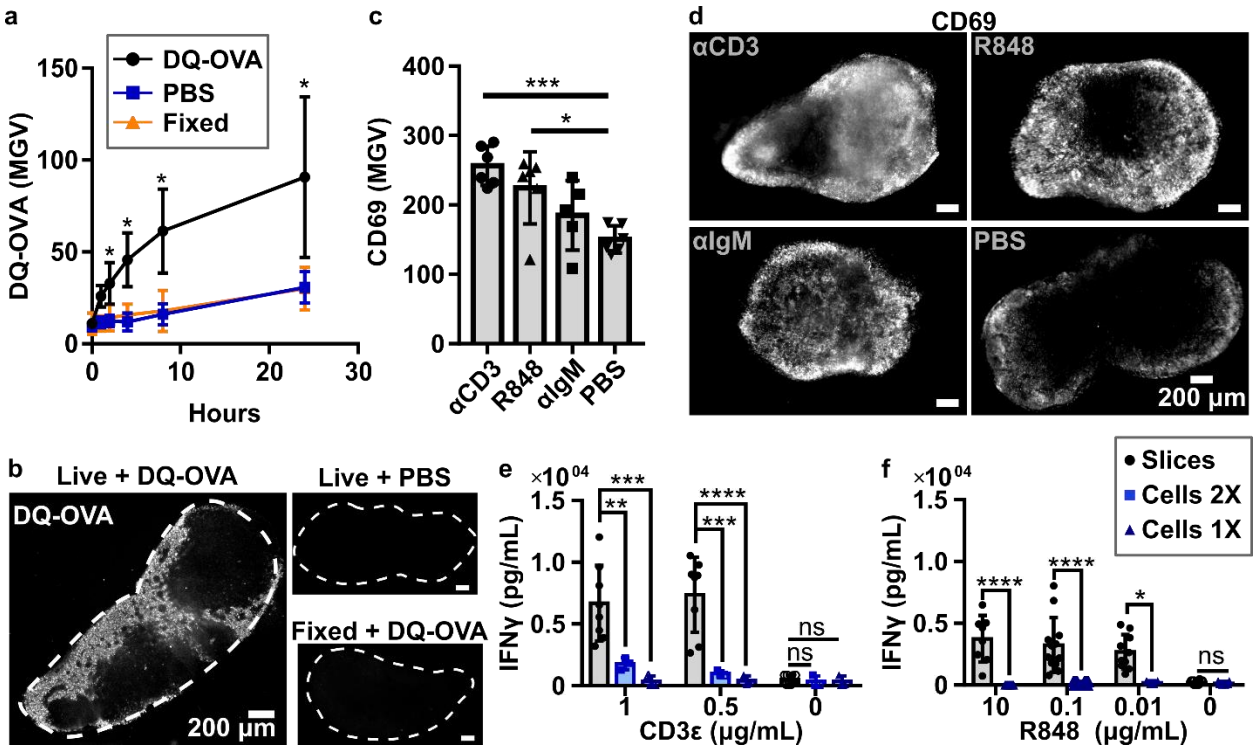

Figure 5: Slices processed protein antigen and responded to cellular stimulation (a) Mean fluorescent intensity of DQ-OVA in lymph slices, showing processing of this protein antigen. Statistically significant increases in intensity compared to controls were seen in live slices cultured with DQ-OVA after only 2 hours of culture. Live slices incubated with 1x PBS and fixed slices incubated with DQ-OVA were used as negative controls. 2-way ANOVA with multiple comparisons. N = 9 slices *p<0.05. (b) Representative images of slices from (a) after 4 hours of culture. Slices outlined with dashed white line. (c) Mean surface expression of CD69 was increased after 24-hour stimulation with α-CD3 or R848. One-way ANOVA with multiple comparisons. Each dot represents one slice; ***p=0.0005, *p=0.0110. (d) Representative images of slices from (c), showing localization of CD69 staining. (e,f) IFNγ secretion from slices and mixed lymphocyte culture after 20-hour direct (CD3ε, e) or indirect (R848, f) T cell stimulation. Lymphocyte concentration was matched to LN slice, 1X: 1.7 x10^6 cells/mL, 2X: 3.4 x10^6 cells/mL. (e) IFNγ secretion after 20-hr stimulation with CD3Ɛ. Dark grey points represent data that was set to the limit of detection for the plate. (f) IFNγ secretion after 20-hr stimulation with R848. Each dot represents one slice/cell culture. N = 6-12 slices and 3-4 cell cultures. Error bars denote standard deviation. 2-way ANOVA with Sidaks multiple comparisons. *p=0.0102, **p=0.0029, ***p=.00001, ****p<0.0001, n.s. denotes p>0.05.

We next tested the extent to which lymph node slices are able to respond to the activation of T cells (anti-CD3, TCR engagement), B cells (anti-IgM, BCR engagement) and APCs (R848, a TLR7 agonist)[84–86]. Statistically significant increases in CD69 surface staining were induced by anti-CD3 and

R848 but not anti-IgM (Figure 5 c). Notably, anti-CD3 elicited these responses without inclusion of anti-CD28, suggesting that the co-stimulatory signal was adequately provided by the CD80/86 on APCs present within the tissue slice. CD69 expression was higher after anti-CD3 stimulation than after R848 stimulation; we hypothesize this is due to the different mechanisms of action. Anti-CD3 cross-links the TCR directly activating the T cells, while R848 acts on T cells indirectly by activating APCs to produce IL-12 that then stimulates nearby T cells.[87,88] The staining pattern also reflected these differences (Figure 5 d, Figure S4). All slices, including unstimulated controls, showed CD69 signal around the perimeter of the tissue. Slices stimulated with anti-CD3 or R848 both had elevated expression within cortical regions of the lymph node, which are rich in both B cells and T cells, but R848-stimulated slices consistently lacked CD69 signal in the T cell-rich center.[89,90] Anti-IgM stimulation resulted in an uniform staining pattern but with much lower average intensity over the entire slice.

We further tested the response to anti-CD3 and R848 in terms of cytokine secretion after overnight culture, and directly compared the response of lymph node slices to lymphocyte suspensions at matched cell densities. As expected, both tissue slices and cell cultures responded to anti-CD3 with IFN-γ and IL-2 secretion, and unstimulated samples did not secrete measurable IFN-γ or IL-2 (Figure 5 e, Figure S5). Interestingly, we observed up to an 18-fold increase in IFN-γ but not IL-2 secretion in tissue slices compared to cell culture. We speculate that the integrity of lymphocyte contacts with stromal cells and antigen-presenting cells (e.g. providing CD28 ligation), as well as the intact profile of secreted factors, may play a role in differences between slices and cells. These data are consistent with prior reports that sliced human tonsil and spleen respond to stimulation with a different cytokine profile than matched tonsil cell or splenocyte cultures.[52,91] Similarly, stimulation with R848 also resulted in an statistically significant increased IFN-γ production compared to lymphocyte culture (Figure 5 f). In fact, the lymphocyte response to these concentrations of R848 was very weak, possibly due to the relative scarcity of matrix-bound APCs in lymphocyte cell cultures.[92,93] Splenocyte culture has a higher population of APCs compared to lymphocytes, and splenocytes did have a detectable response to R848 (Figure S6).[94,95] From these data, we conclude that tissue slices can respond to ex vivo stimulation with both surface marker upregulation and cytokine secretion. By keeping the cells in the same organization that they are in vivo, slices maintain cellular interactions that are not seen in vitro.

Live lymph node slices responded to antigen-specific challenge.

Finally, we tested the ability of lymph node slices to recall an antigen-specific response ex vivo. In vivo vaccination elicits a complex series of responses, including antigen trafficking and processing, cellular activation, and cytokine secretion, at specific times that reflect the ongoing development of the adaptive immune response. Here we tested a subset of these readouts to assess the ability of ex vivo lymph node slices to report on this in vivo activity. Taking advantage of the OVA/OTII model antigen system, mice received OVA-transgenic CD4+ T cells (OTII) intravenously, then were primed subcutaneously with either a model vaccine (alum and OVA protein) or a vehicle control (PBS) (Figure 6 a). In this system we expected to measure adjuvant-mediated and initial T cell responses between days 1 and 4, with a full T cell response by day 7.[96] Alum vaccines are known to produce a Th2-skewed response, and we expected to see this polarization in our slice culture system in the form of IL-4 secretion.[97,98]

Because activated APCs may decrease their phagocytic properties,[99] we first tested whether cells in lymph node slices from vaccinated mice were able to process DQ-OVA on this time scale. Unexpectedly, DQ-OVA processing in these slices was unchanged compared to slices from control animals (Figure 6 b). We speculate that the unaltered processing of DQ-OVA in the lymph node may due to the presence of lymph-node resident DCs that were not activated by the s.c. alum injection. This result indicated that ex vivo incubation with antigen would still be effective in lymph node slices from vaccinated animals.

To quantify early and late responses to vaccination, lymph nodes were collected on days 1, 4, and 7 after vaccination, sliced, and cultured for 24-hr in the presence or absence of OVA protein in the media. TNFα secretion was not detectable at any time point (Figure 6 c), consistent with other reports for alum adjuvants.[100,97] By day 4, a strong antigen-specific IFNγ response was detected in slices from vaccinated animals (Figure 6 d). Slices from control animals did not secrete IFNγ upon ex vivo culture with OVA, confirming that the response arose from vaccination. Consistent with the timing of the IFNγ response, on day 4 we also observed a significant increase in CD69 surface marker immunofluorescence in vaccinated/restimulated slices compared to vaccinated/unstimulated and vehicle controls (Figure 6 f).

CD69 upregulation was located throughout the slice (Figure 6 g, Figure S7). No CD69 upregulation was detected on days 1 or 7 (not shown). As expected for an alum-adjuvanted vaccine,[96,98] we observed a statistically significant increase in antigen-specific IL-4 production in lymph node slices from vaccinated animals (Figure 6 e). Interestingly, the peak days for IFN-γ and IL-4 differed (days 4 and 7, respectively), suggesting an evolution of the in vivo immune response. In summary, these data provide compelling evidence that murine lymph node slices can mount antigen-specific responses ex vivo, including to intact protein antigens. Slice cultures simultaneously yielded data on the timing of cytokine secretion and the distribution of immunofluorescence staining, and could match trends across the results. Overall these data show the versatility of live lymph node tissue slices to provide multiple readouts and potentially serve as an ex vivo model of immunity.

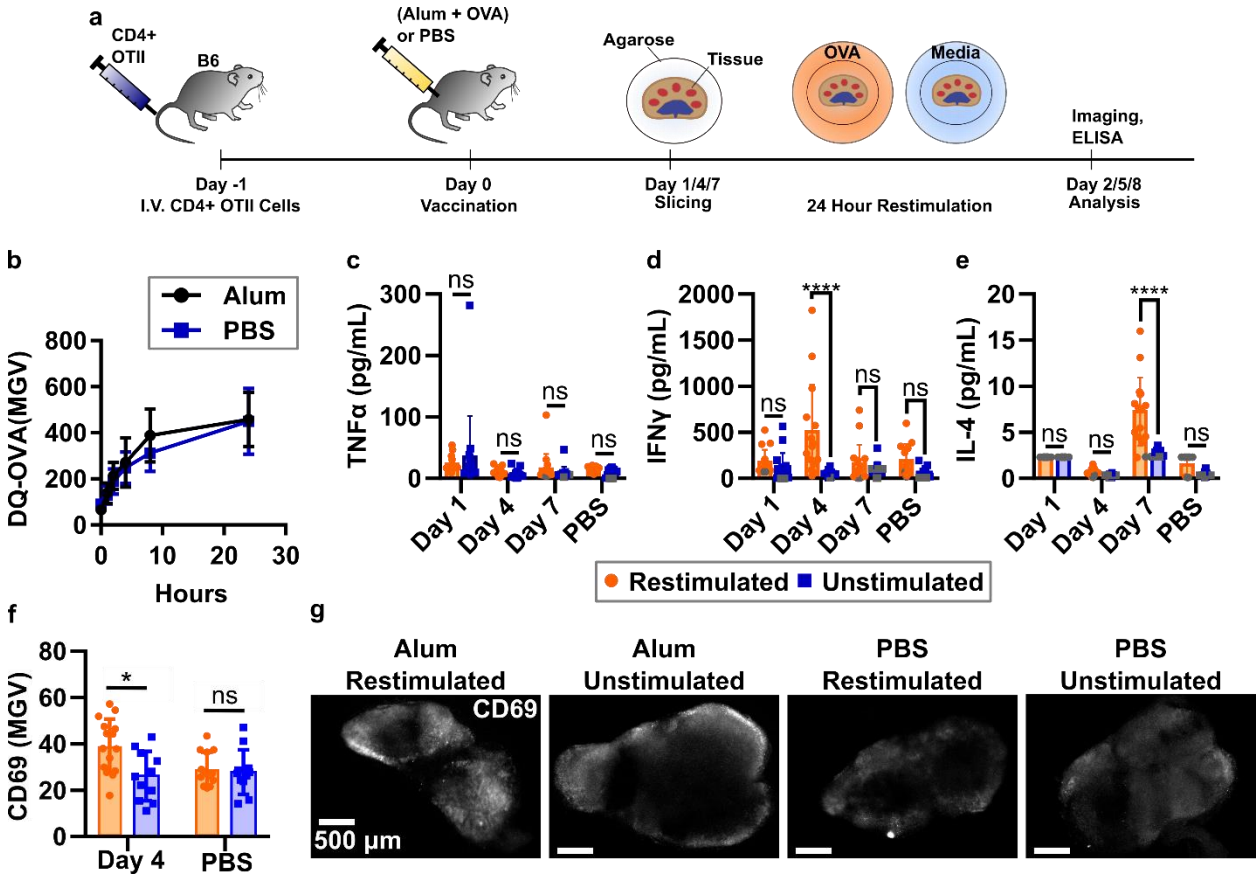

Figure 6: Lymph node slices showed antigen-specific stimulation after vaccination. (a) Schematic of experimental procedure. Black/6 mice were given CD4+ OTII cells IV and rested one day before vaccination with either alum and OVA protein or PBS. Tissues were collected on 1, 4, and 7 days after vaccination and sliced. Slices were then cultured with or without OVA protein challenge for 24 hours. Cytokine analysis was completed by ELISA from surrounding media and slices were immunostained for activation markers. (b) Slices from mice vaccinated with alum+OVA four days prior processed OVA

antigen at the same rate as those from unvaccinated mice. N=12 slices. (c-d) Quantification of cytokine secretion into the culture media after 24-hr culture with or without OVA. Antigen-specific IFN-γ response was detected on day 4; antigen-specific IL-2 response was detected on day 7. Dark grey points represent data that was set at the limit of detection for the plate. (f) Antigen-specific CD69 upregulation was seen on day 4. (g) Representative images from (f). Slices were stained with FITC-B220 and AF647-CD69. Scalebars all 500 μm. Each dot represents a single slice with bars indicating mean ± standard deviation. Two-way ANOVA with multiple comparisons. *$p<0.05$, **$p<0.01$

Discussion:

The data in this paper lay out a set of best practices for slicing murine lymph nodes and maintaining them in 24-hr culture, and demonstrate that slices have the potential to be used for studying T cell activation and antigen-specific responses. Slices retained viability for 24 hours in culture and did not show signs of inflammation. Slices retained the spatial organization seen in vivo while making the tissue readily accessible for imaging and immunostaining, offering the potential to easily image cellular interactions, motility, and changes in surface marker expression during culture. Lymph node slices offered a cytokine response that differed in some cases from lymphocyte culture, consistent with prior reports for other lymphoid tissues.[48,52] This may reflect the intact extracellular environment and cell-cell interactions that would be found in vivo. Most interestingly, this work provided evidence that lymph node slices could be used to report antigen-specific responses to vaccination, while offering the ability for multi-modal readout that combines imaging and traditional analysis such as ELISA and flow cytometry. Overall, this work lays the foundation for lymph node slices to serve as a controlled, ex vivo experimental platform in which to study the spatial organization and dynamics of the lymph node.

Traditionally, antigen presentation studies have been conducted by in vitro cell culture or by in vivo imaging, frequently using DCs pulsed with protein or peptide antigen.[68,71] By using intact tissue ex vivo instead of co-culturing T cells with DCs in vitro, the contributions other cell types are retained, e.g. fibroblastic reticular cells (FRCs), with which T cells interact with at a higher frequency than with DCs.[101] We note that pulsed DC cultures could, in principle, be overlaid onto ex vivo lymph node slices for facile imaging of T cell-DC interactions similar to the in vivo studies, although overlays would not produce the fine segregation of DC phenotypes seen in vivo.[68,71,93] Here, the lymph node was primed in vivo, then challenged ex vivo with antigen in a manner similar to traditional ELIspot assays. The finding that cells in LN slices were able to process protein antigen for antigen-specific T cell activation opens the possibility

for ex vivo analysis of intercellular interactions as well as antigenicity analysis. In contrast, peptides may load onto any available MHC, potentially introducing cellular interactions that would not traditionally occur. Furthermore, antigen-presenting cells were presumably present in same numbers and locations as they were in vivo.

Like any model system, ex vivo platforms have inherent limitations that impact experimental design. Once the tissue has been removed from the body, no additional cells can be recruited from other areas such as memory B cells from the bone marrow or circulating T cells from the blood stream.[102,103] However, cells can be overlaid onto the slice ex vivo at known concentrations and times.[46,54] Removal from the body also eliminates blood, lymphatic, and interstitial fluid flow, so shear stress is altered compared to what the organ feels in vivo. This limitation is also present in standard lymphocyte cultures, and may have an impact on stromal cells in particular.[104] Flow can be introduced into the system either through the tissue by gravity, or across the tissue with pumps.[64] These flow rates can be altered to mimic different disease states in vivo and offer greater control of the experimental system. Microfluidics can offer a controlled approach for both the perfusion of tissue and potentially long-term culture.[105–107] Finally, drugs, cells, and other stimuli added to the culture media over a lymph node slice can enter the entire cut surface of the tissue, rather than being restricted to enter through the lymphatic or blood vasculature. This means that ex vivo slice treatment should not be used to report in vivo biodistribution, although uptake may still be somewhat selective based on regional cell activity (e.g. DQ-OVA uptake in Figure 5 b, and regional T cell homing reported previously[54]). Looking ahead, it will be useful to increase the longevity of the cultures to several days or weeks, to monitor an immune response from onset to completion ex vivo. Long term culture poses several challenges, including nutrient supplementation and oxygenation of the tissue, as well as retention of motile lymphocytes within the slices. As they currently stand, lymph node slices are able to provide valuable insight into short-term immune functions.

We are optimistic that live lymph node slices will provide a novel platform that will add to the immunologist's tool box as a supplement to traditional experimental models, providing a new angle of investigation based on spatially organized and dynamic cell-cell and cell-matrix interactions, coupled with the responses to well defined ex vivo stimulation. The enduring success of brain, lung, and tumor slices to

study cellular and tissue-level events, pharmacological responses, and even response to damage and infection, indicates the wide array of potential utility for lymph node slices. Indeed, human tonsil slices are already in use in this manner.[51,108] Lymph node slices may also prove useful for monitoring the effect the immune system can have on similar culture systems, e.g. by co-culturing lymph node tissue with tissues from other organs.[64] In summary, the methods for collecting and working with acute murine lymph node slices presented here provide a basis for the use of this model system to study dynamics and cellular interactions; applications may span the range of vaccine development, infectious disease, cancer immunity, and autoimmunity.

Conflict of Interest Statement

The authors have no conflicts of interest to declare.

Acknowledgements

The authors thank the Hartwell Foundation for supporting this work. Research reported in this publication was also supported by the National Institute of Allergy and Infectious Diseases under Award Number R01AI131723 through the National Institutes of Health. M. C. Belanger was supported in part by the Immunology Training Grant at the University of Virginia (NIH, 5T32AI007496-23). The content is solely the responsibility of the authors and does not necessarily represent the official views of the National Institutes of Health. Finally, the authors acknowledge the Flow Cytometry Core and the W.M. Keck center for cellular imaging at the University of Virginia for their technical expertise.

References

1 Qi H, Kastenmüller W, Germain RN. Spatiotemporal Basis of Innate and Adaptive Immunity in Secondary Lymphoid Tissue. *Annu Rev Cell Dev Biol* 2014; **30**: 141–167.

2 Gaylo A, Schrock DC, Fernandes NRJ, Fowell DJ. T Cell Interstitial Migration: Motility Cues from the Inflamed Tissue for Micro- and Macro-Positioning. *Front Immunol* 2016; **7**. doi:10.3389/fimmu.2016.00428.

3 Gonzalez SF, Pitcher LA, Mempel T, Schuerpf F, Carroll MC. B cell acquisition of antigen in vivo. *Curr Opin Immunol* 2009; **21**: 251–257.

4 Willard-Mack CL. Normal Structure, Function, and Histology of Lymph Nodes. *Toxicol Pathol* 2006; **34**: 409–424.

5 Thurley K, Gerecht D, Friedmann E, Höfer T. Three-Dimensional Gradients of Cytokine Signaling between T Cells. *PLoS Comput Biol* 2015; **11**. doi:10.1371/journal.pcbi.1004206.

6 Lian J, Luster AD. Chemokine-guided cell positioning in the lymph node orchestrates the generation of adaptive immune responses. *Curr Opin Cell Biol* 2015; **36**: 1–6.

7 Vaday GG, Lider O. Extracellular matrix moieties, cytokines, and enzymes: dynamic effects on immune cell behavior and inflammation. *J Leukoc Biol* 2000; **67**: 149–159.

8 Schmitz ML, Weber A, Roxlau T, Gaestel M, Kracht M. Signal integration, crosstalk mechanisms and networks in the function of inflammatory cytokines. *Biochim Biophys Acta BBA - Mol Cell Res* 2011; **1813**: 2165–2175.

9 Germain RN, Bajénoff M, Castellino F, Chieppa M, Egen JG, Huang AYC *et al.* Making friends in out-of-the-way places: how cells of the immune system get together and how they conduct their business as revealed by intravital imaging. *Immunol Rev* 2008; **221**: 163–181.

10 Kastenmüller W, Torabi-Parizi P, Subramanian N, Lämmermann T, Germain RN. A Spatially-Organized Multicellular Innate Immune Response in Lymph Nodes Limits Systemic Pathogen Spread. *Cell* 2012; **150**: 1235–1248.

11 Pompano RR, Chiang AH, Kastrup CJ, Ismagilov RF. Conceptual and Experimental Tools to Understand Spatial Effects and Transport Phenomena in Nonlinear Biochemical Networks Illustrated with Patchy Switching. 2017; **86**: 333–356.

12 Saeys Y, Van Gassen S, Lambrecht BN. Computational flow cytometry: helping to make sense of high-dimensional immunology data. *Nat Rev Immunol* 2016; **16**: 449–462.

13 Spitzer MH, Nolan GP. Mass Cytometry: Single Cells, Many Features. *Cell* 2016; **165**: 780–791.

14 Faley S, Seale K, Hughey J, Schaffer DK, VanCompernolle S, McKinney B *et al.* Microfluidic platform for real-time signaling analysis of multiple single T cells in parallel. *Lab Chip* 2008; **8**: 1700–1712.

15 Ogunniyi AO, Thomas BA, Politano TJ, Varadarajan N, Landais E, Poignard P *et al.* Profiling human antibody responses by integrated single-cell analysis. *Vaccine* 2014; **32**: 2866–2873.

16 Han Q, Bradshaw EM, Nilsson B, Hafler DA, Love JC. Multidimensional analysis of the frequencies and rates of cytokine secretion from single cells by quantitative microengraving. *Lab Chip* 2010; **10**: 1391.

17 Xue Q, Lu Y, Eisele MR, Sulistijo ES, Khan N, Fan R *et al.* Analysis of single-cell cytokine secretion reveals a role for paracrine signaling in coordinating macrophage responses to TLR4 stimulation. *Sci Signal* 2015; **8**: ra59.

18 Chattopadhyay PK, Gierahn TM, Roederer M, Love JC. Single-cell technologies for monitoring immune systems. *Nat Immunol* 2014; **15**: 128–135.

19 Shalek AK, Satija R, Shuga J, Trombetta JJ, Gennert D, Lu D *et al.* Single-cell RNA-seq reveals dynamic paracrine control of cellular variation. *Nature* 2014; **510**: 363–369.

20 Consortium TTM, Quake SR, Wyss-Coray T, Darmanis S. Transcriptomic characterization of 20 organs and tissues from mouse at single cell resolution creates a Tabula Muris. *bioRxiv* 2017; : 237446.

21 Everts B. Metabolomics in Immunology Research. *Methods Mol Biol Clifton NJ* 2018; **1730**: 29–42.

22 Wu M, Neilson A, Swift AL, Moran R, Tamagnine J, Parslow D *et al.* Multiparameter metabolic analysis reveals a close link between attenuated mitochondrial bioenergetic function and enhanced glycolysis dependency in human tumor cells. *Am J Physiol Cell Physiol* 2007; **292**: C125-136.

23 Shakhar G, Lindquist RL, Skokos D, Dudziak D, Huang JH, Nussenzweig MC *et al.* Stable T cell-dendritic cell interactions precede the development of both tolerance and immunity in vivo. *Nat Immunol* 2005; **6**: 707–714.

24 Matheu MP, Parker I, Cahalan MD. Dissection and 2-Photon Imaging of Peripheral Lymph Nodes in Mice. *J Vis Exp JoVE* 2007. doi:10.3791/265.

25 Liu Z, Gerner MY, Panhuys NV, Levine AG, Rudensky AY, Germain RN. Immune homeostasis enforced by co-localized effector and regulatory T cells. *Nature* 2015; **528**: 225–230.

26 Germain RN, Robey EA, Cahalan MD. A Decade of Imaging Cellular Motility and Interaction Dynamics in the Immune System. *Science* 2012; **336**: 1676–1681.

27 Dzhagalov IL, Melichar HJ, Ross JO, Herzmark P, Robey EA. Two-photon imaging of the immune system. *Curr Protoc Cytom Editor Board J Paul Robinson Manag Ed Al* 2012; **Chapter 12**: Unit12.26.

28 Rodda LB, Lu E, Bennett ML, Sokol CL, Wang X, Luther SA *et al.* Single-Cell RNA Sequencing of Lymph Node Stromal Cells Reveals Niche-Associated Heterogeneity. *Immunity* 2018; **48**: 1014-1028.e6.

29 Goltsev Y, Samusik N, Kennedy-Darling J, Bhate S, Hale M, Vazquez G *et al.* Deep Profiling of Mouse Splenic Architecture with CODEX Multiplexed Imaging. *Cell* 2018; **174**: 968-981.e15.

30 Stoler-Barak L, Biram A, Davidzohn N, Addadi Y, Golani O, Shulman Z. B cell dissemination patterns during the germinal center reaction revealed by whole-organ imaging. *J Exp Med* 2019; **216**: 2515–2530.

31 Gosselin EA, Eppler HB, Bromberg JS, Jewell CM. Designing natural and synthetic immune tissues. *Nat Mater* 2018; **17**: 484–498.

32 Allen CDC, Cyster JG. Follicular dendritic cell networks of primary follicles and germinal centers: phenotype and function. *Semin Immunol* 2008; **20**: 14–25.

33 Fletcher AL, Acton SE, Knoblich K. Lymph node fibroblastic reticular cells in health and disease. *Nat Rev Immunol* 2015; **15**: 350–361.

34 Chang JE, Turley SJ. Stromal infrastructure of the lymph node and coordination of immunity. *Trends Immunol* 2015; **36**: 30–39.

35 Gerner MY, Kastenmuller W, Ifrim I, Kabat J, Germain RN. Histo-Cytometry: A Method for Highly Multiplex Quantitative Tissue Imaging Analysis Applied to Dendritic Cell Subset Microanatomy in Lymph Nodes. *Immunity* 2012; **37**: 364–376.

36 Manifold MC. The Effect of Certain Antiseptics on the Respiration of Brain Tissues in vitro. *Br J Exp Pathol* 1941; **22**: 111–126.

37 Rafaelsen OJ. Action of Insulin on Glucose Uptake of Rat Brain Slices and Isolated Rat Cerebellum. *J Neurochem* 1961; **7**: 45–51.

38 Yamamoto C, McIlwain H. Electrical Activities in Thin Sections from the Mammalian Brain Maintained in Chemically-Defined Media in Vitro. *J Neurochem* 1966; **13**: 1333–1343.

39 Collingridge GL. The brain slice preparation: a tribute to the pioneer Henry McIlwain. *J Neurosci Methods* 1995; **59**: 5–9.

40 Buskila Y, Breen PP, Tapson J, Schaik A van, Barton M, Morley JW. Extending the viability of acute brain slices. *Sci Rep* 2014; **4**: 5309.

41 De Simoni A, MY Yu L. Preparation of organotypic hippocampal slice cultures: interface method. *Nat Protoc* 2006; **1**: 1439–1445.

42 Marciniak A, Cohrs CM, Tsata V, Chouinard JA, Selck C, Stertmann J *et al.* Using pancreas tissue slices for in situ studies of islet of Langerhans and acinar cell biology. *Nat Protoc* 2014; **9**: 2809–2822.

43 Olinga P, Schuppan D. Precision-cut liver slices: a tool to model the liver ex vivo. *J Hepatol* 2013; **58**: 1252–1253.

44 Henjakovic M, Sewald K, Switalla S, Kaiser D, Müller M, Veres TZ *et al.* Ex vivo testing of immune responses in precision-cut lung slices. *Toxicol Appl Pharmacol* 2008; **231**: 68–76.

45 Wang K, Lee P, Mirams GR, Sarathchandra P, Borg TK, Gavaghan DJ *et al.* Cardiac tissue slices: preparation, handling, and successful optical mapping. *Am J Physiol - Heart Circ Physiol* 2015; **308**: H1112–H1125.

46 Ross JO, Melichar HJ, Halkias J, Robey EA. Studying T Cell Development in Thymic Slices. *Methods Mol Biol Clifton NJ* 2016; **1323**: 131–140.

47 Lancaster JN, Ehrlich LIR. Analysis of Thymocyte Migration, Cellular Interactions, and Activation by Multiphoton Fluorescence Microscopy of Live Thymic Slices. *Methods Mol Biol Clifton NJ* 2017; **1591**: 9–25.

48 Hoffmann P, Skibinski G, James K. Organ culture of human lymphoid tissue. I. Characteristics of the system. *J Immunol Methods* 1995; **179**: 37–49.

49 Skibinski G, Hoffmann P, Radbruch A, James K. Organ culture of human lymphoid tissue. II. Marked differences in cytokine production and proliferation between slice and suspension cultures of human spleen. *J Immunol Methods* 1997; **205**: 115–125.

50 Knoblich K, Cruz Migoni S, Siew SM, Jinks E, Kaul B, Jeffery HC *et al.* The human lymph node microenvironment unilaterally regulates T-cell activation and differentiation. *PLOS Biol* 2018; **16**: e2005046.

51 Grivel J-C, Margolis L. Use of human tissue explants to study human infectious agents. *Nat Protoc* 2009; **4**: 256–269.

52 Giger B, Bonanomi A, Odermatt B, Ladell K, Speck RF, Kojic D *et al.* Human tonsillar tissue block cultures differ from autologous tonsillar cell suspension cultures in lymphocyte subset activation and cytokine gene expression. *J Immunol Methods* 2004; **289**: 179–190.

53 Asperti-Boursin F, Real E, Bismuth G, Trautmann A, Donnadieu E. CCR7 ligands control basal T cell motility within lymph node slices in a phosphoinositide 3–kinase– independent manner. *J Exp Med* 2007; **204**: 1167–1179.

54 Salmon H, Rivas-Caicedo A, Asperti-Boursin F, Lebugle C, Bourdoncle P, Donnadieu E. Ex vivo Imaging of T Cells in Murine Lymph Node Slices with Widefield and Confocal Microscopes. *J Vis Exp JoVE* 2011; : e3054.

55 Katakai T, Habiro K, Kinashi T. Dendritic Cells Regulate High-Speed Interstitial T Cell Migration in the Lymph Node via LFA-1/ICAM-1. *J Immunol* 2013; **191**: 1188–1199.

56 Katakai T, Kondo N, Ueda Y, Kinashi T. Autotaxin Produced by Stromal Cells Promotes LFA-1–Independent and Rho-Dependent Interstitial T Cell Motility in the Lymph Node Paracortex. *J Immunol* 2014; **193**: 617–626.

57 Katakai T. Live Imaging of Interstitial T Cell Migration Using Lymph Node Slices. In: Ishii M (ed). *Intravital Imaging of Dynamic Bone and Immune Systems : Methods and Protocols*. Springer New York: New York, NY, 2018, pp 29–42.

58 Mohammed JS, Caicedo HH, Fall CP, Eddington DT. Microfluidic add-on for standard electrophysiology chambers. *Lab Chip* 2008; **8**: 1048–1055.

59 Salmon H, Rivas-Caicedo A, Asperti-Boursin F, Lebugle C, Bourdoncle P, Donnadieu E. Ex vivo Imaging of T Cells in Murine Lymph Node Slices with Widefield and Confocal Microscopes. *J Vis Exp* 2011. doi:10.3791/3054.

60 Ross AE, Belanger MC, Woodroof JF, Pompano RR. Spatially resolved microfluidic stimulation of lymphoid tissue ex vivo. *Analyst* 2017; **142**: 649–659.

61 Groff BD, Kinman AWL, Woodroof JF, Pompano RR. Immunofluorescence staining of live lymph node tissue slices. *J Immunol Methods* 2018. doi:10.1016/j.jim.2018.10.010.

62 Ross AE, Pompano RR. Diffusion of cytokines in live lymph node tissue using microfluidic integrated optical imaging. *Anal Chim Acta* 2018; **1000**: 205–213.

63 Ross JennyO, Melichar HeatherJ, Halkias J, Robey EllenA. Studying T Cell Development in Thymic Slices. In: Bosselut R, S. Vacchio M, Vacchio MS (eds). *T-Cell Development*. Springer New York, 2016, pp 131–140.

64 Shim S, Belanger MC, Harris AR, Munson JM, Pompano RR. Two-way communication between ex vivo tissues on a microfluidic chip: application to tumor-lymph node interaction. *Lab Chip* 2019; **19**: 1013–1026.

65 Schneider CA, Rasband WS, Eliceiri KW. NIH Image to ImageJ: 25 years of image analysis. *Nat Methods* 2012; **9**: 671–675.

66 Asperti-Boursin F, Real E, Bismuth G, Trautmann A, Donnadieu E. CCR7 ligands control basal T cell motility within lymph node slices in a phosphoinositide 3–kinase– independent manner. *J Exp Med* 2007; **204**: 1167–1179.

67 Gerner MY, Kastenmuller W, Ifrim I, Kabat J, Germain RN. Histo-Cytometry: A Method for Highly Multiplex Quantitative Tissue Imaging Analysis Applied to Dendritic Cell Subset Microanatomy in Lymph Nodes. *Immunity* 2012; **37**: 364–376.

68 Stoll S, Delon J, Brotz TM, Germain RN. Dynamic Imaging of T Cell-Dendritic Cell Interactions in Lymph Nodes. *Science* 2002; **296**: 1873–1876.

69 Garside P. Visualization of Specific B and T Lymphocyte Interactions in the Lymph Node. *Science* 1998; **281**: 96–99.

70 Moran I, Nguyen A, Khoo WH, Butt D, Bourne K, Young C *et al.* Memory B cells are reactivated in subcapsular proliferative foci of lymph nodes. *Nat Commun* 2018; **9**. doi:10.1038/s41467-018-05772-7.

71 Malide D. In Vivo Cell Tracking Using Two-Photon Microscopy. In: Bai M (ed). *In Vivo Fluorescence Imaging: Methods and Protocols*. Springer New York: New York, NY, 2016, pp 109–122.

72 Bajénoff M, Egen J, Koo LY, Laugier JP, Brau F, Glaichenhaus N *et al.* Stromal Cell Networks Regulate Lymphocyte Entry, Migration, and Territoriality in Lymph Nodes. *Immunity* 2006; **25**: 989–1001.

73 Hume DA. Macrophages as APC and the Dendritic Cell Myth. *J Immunol* 2008; **181**: 5829–5835.

74 Craston R, Koh M, Mc Dermott A, Ray N, Prentice HG, Lowdell MW. Temporal dynamics of CD69 expression on lymphoid cells. *J Immunol Methods* 1997; **209**: 37–45.

75 Dilioglou S, Cruse JM, Lewis RE. Function of CD80 and CD86 on monocyte- and stem cell-derived dendritic cells. *Exp Mol Pathol* 2003; **75**: 217–227.

76 Sahoo NC, Rao KVS, Natarajan K. CD80 expression is induced on activated B cells following stimulation by CD86. *Scand J Immunol* 2002; **55**: 577–584.

77 Astolfi M, Péant B, Lateef MA, Rousset N, Kendall-Dupont J, Carmona E *et al.* Micro-dissected tumor tissues on chip: an ex vivo method for drug testing and personalized therapy. *Lab Chip* 2016; **16**: 312–325.

78 Graaf IAM de, Meijeren CE van, Pektaş F, Koster HJ. Comparison of in Vitro Preparations for Semi-Quantitative Prediction of in Vivo Drug Metabolism. *Drug Metab Dispos* 2002; **30**: 1129–1136.

79 Graaf IAM de, Olinga P, Jager MH de, Merema MT, Kanter R de, Kerkhof EG van de *et al.* Preparation and incubation of precision-cut liver and intestinal slices for application in drug metabolism and toxicity studies. *Nat Protoc* 2010; **5**: 1540–1551.

80 Zenewicz LA. Oxygen Levels and Immunological Studies. *Front Immunol* 2017; **8**. doi:10.3389/fimmu.2017.00324.

81 Buskila Y, Breen PP, Tapson J, van Schaik A, Barton M, Morley JW. Extending the viability of acute brain slices. *Sci Rep* 2014; **4**: 5309.

82 Papouin T, Haydon PG. Obtaining Acute Brain Slices. *Bio-Protoc* 2018; **8**. doi:10.21769/BioProtoc.2699.

83 Davies EJ, Dong M, Gutekunst M, Närhi K, van Zoggel HJAA, Blom S *et al.* Capturing complex tumour biology *in vitro*: histological and molecular characterisation of precision cut slices. *Sci Rep* 2015; **5**: 17187.

84 Wagner TL, Ahonen CL, Couture AM, Gibson SJ, Miller RL, Smith RM *et al.* Modulation of TH1 and TH2 cytokine production with the immune response modifiers, R-848 and imiquimod. *Cell Immunol* 1999; **191**: 10–19.

85 Tomai MA, Imbertson LM, Stanczak TL, Tygrett LT, Waldschmidt TJ. The immune response modifiers imiquimod and R-848 are potent activators of B lymphocytes. *Cell Immunol* 2000; **203**: 55–65.

86 Jurk M, Heil F, Vollmer J, Schetter C, Krieg AM, Wagner H *et al.* Human TLR7 or TLR8 independently confer responsiveness to the antiviral compound R-848. *Nat Immunol* 2002; **3**: 499.

87 Rubtsova K, Rubtsov AV, Halemano K, Li SX, Kappler JW, Santiago ML *et al.* T Cell Production of IFNγ in Response to TLR7/IL-12 Stimulates Optimal B Cell Responses to Viruses. *PLoS ONE* 2016; **11**. doi:10.1371/journal.pone.0166322.

88 Caron G, Duluc D, Frémaux I, Jeannin P, David C, Gascan H *et al.* Direct Stimulation of Human T Cells via TLR5 and TLR7/8: Flagellin and R-848 Up-Regulate Proliferation and IFN-γ Production by Memory CD4+ T Cells. *J Immunol* 2005; **175**: 1551–1557.

89 Hugues S, Fetler L, Bonifaz L, Helft J, Amblard F, Amigorena S. Distinct T cell dynamics in lymph nodes during the induction of tolerance and immunity. *Nat Immunol* 2004; **5**: 1235–1242.

90 Mempel TR, Henrickson SE, von Andrian UH. T-cell priming by dendriticcells in lymph nodes occurs in three distinct phases. *Nature* 2004; **427**: 154–159.

91 Hoffmann P, Skibinski G, James K. Organ culture of human lymphoid tissue. I. Characteristics of the system. *J Immunol Methods* 1995; **179**: 37–49.

92 Parmentier HK, van der Linden JA, Krijnen J, van Wichen DF, Rademakers LH, Bloem AC *et al.* Human follicular dendritic cells: isolation and characteristics in situ and in suspension. *Scand J Immunol* 1991; **33**: 441–452.

93 Gerner MY, Kastenmuller W, Ifrim I, Kabat J, Germain RN. Histo-cytometry: a method for highly multiplex quantitative tissue imaging analysis applied to dendritic cell subset microanatomy in lymph nodes. *Immunity* 2012; **37**: 364–376.

94 Shen E, Lu L, Wu C. TLR7/8 ligand, R-848, inhibits IgE synthesis by acting directly on B lymphocytes. *Scand J Immunol* 2008; **67**: 560–568.

95 Wang X, Li L, Wang J, Dong L, Shu Y, Liang Y *et al.* Inhibition of cytokine response to TLR stimulation and alleviation of collagen-induced arthritis in mice by Schistosoma japonicum peptide SJMHE1. *J Cell Mol Med* 2017; **21**: 475–486.

96 Kim C, Fang F, Weyand CM, Goronzy JJ. The life cycle of a T cell after vaccination – where does immune ageing strike? *Clin Exp Immunol* 2017; **187**: 71–81.

97 Orr MT, Khandhar AP, Seydoux E, Liang H, Gage E, Mikasa T *et al.* Reprogramming the adjuvant properties of aluminum oxyhydroxide with nanoparticle technology. *Npj Vaccines* 2019; **4**: 1–10.

98 Kool M, Fierens K, Lambrecht BN. Alum adjuvant: some of the tricks of the oldest adjuvant. *J Med Microbiol* 2012; **61**: 927–934.

99 Trombetta ES, Mellman I. Cell Biology of Antigen Processing in Vitro and in Vivo. *Annu Rev Immunol* 2005; **23**: 975–1028.

100 Mosca F, Tritto E, Muzzi A, Monaci E, Bagnoli F, Iavarone C *et al.* Molecular and cellular signatures of human vaccine adjuvants. *Proc Natl Acad Sci* 2008; **105**: 10501–10506.

101 Tasnim H, Fricke GM, Byrum JR, Sotiris JO, Cannon JL, Moses ME. Quantitative Measurement of Naïve T Cell Association With Dendritic Cells, FRCs, and Blood Vessels in Lymph Nodes. *Front Immunol* 2018; **9**. doi:10.3389/fimmu.2018.01571.

102 Shenoy GN, Chatterjee P, Kaw S, Mukherjee S, Rathore DK, Bal V *et al.* Recruitment of Memory B Cells to Lymph Nodes Remote from the Site of Immunization Requires an Inflammatory Stimulus. *J Immunol* 2012; **189**: 521–528.

103 Nolz JC. Molecular Mechanisms of CD8+ T cell Trafficking and Localization. *Cell Mol Life Sci CMLS* 2015; **72**: 2461–2473.

104 Tomei AA, Siegert S, Britschgi MR, Luther SA, Swartz MA. Fluid Flow Regulates Stromal Cell Organization and CCL21 Expression in a Tissue-Engineered Lymph Node Microenvironment. *J Immunol* 2009; **183**: 4273–4283.

105 van Midwoud PM, Groothuis GMM, Merema MT, Verpoorte E. Microfluidic biochip for the perifusion of precision-cut rat liver slices for metabolism and toxicology studies. *Biotechnol Bioeng* 2010; **105**: 184–194.

106 van Midwoud PM, Merema MT, Verpoorte E, Groothuis GMM. A microfluidic approach for in vitro assessment of interorgan interactions in drug metabolism using intestinal and liver slices. *Lab Chip* 2010; **10**: 2778–2786.

107 Komeya M, Kimura H, Nakamura H, Yokonishi T, Sato T, Kojima K *et al.* Long-term ex vivo maintenance of testis tissues producing fertile sperm in a microfluidic device. *Sci Rep* 2016; **6**: 1–10.

108 Davies FJ, Olme C, Lynskey NN, Turner CE, Sriskandan S. Streptococcal superantigen-induced expansion of human tonsil T cells leads to altered T follicular helper cell phenotype, B cell death and reduced immunoglobulin release. *Clin Exp Immunol* 2019; **197**: 83–94.